Algal Research 76 (2023) 103317

Contents lists available at ScienceDirect

Algal Research

journal homepage: www.elsevier.com/locate/algal

Spiral inertial microfluidics for separation and concentration of phytoplankton

Vitor Magalhães [a,c], Vânia Pinto [a,c,*], Paulo Sousa [a,c], Luís Gonçalves [a,c], Emilio Fernández [b], Graça Minas [a,c,*]

[a] CMEMS-UMinho, University of Minho, Campus de Azurém, 4800-058 Guimarães, Portugal
[b] Centro de Investigación Mariña, Faculty of Marine Science, 36310, Universidade de Vigo, Spain
[c] LABBELS –Associate Laboratory, Braga, Guimarães, Portugal

ARTICLE INFO

Keywords:
HABs
Inertial microfluidics
Alexandrium species
Size-based separation
Cell enrichment

ABSTRACT

Harmful algal blooms (HABs) are a recurring phenomenon along all continents, posing a global threat, particularly due to shellfish poisoning and public health, and their timely monitoring is vital for safeguarding the blue economy. The ability to efficiently isolate species of interest, such as harmful dinoflagellates, is a key process for HABs monitoring which is particularly complex because of the typically high diversity of marine microalgae communities. This study introduces a simple spiral microchannel device using inertial microfluidics to separate and concentrate microalgae based on size. This device effectively concentrates microalgae, achieving up to 5.8-fold fluorescence increase after 3 cycles in the spiral and isolates target species with <6 % cell loss. A continuous enrichment method demonstrated a 2.85-fold increase in fluorescence signal for *Alexandrium minutum* after 80 min. This method proved suitable to enhance the sensitivity of devices designed to detect harmful phytoplankton species' early blooms.

1. Introduction

Phytoplankton are a diverse group of microscopic photosynthetic unicellular organisms, with sizes ranging from <1 μm to colonies larger than 500 μm, and are annually responsible for roughly half of the primary production on the planet, being the basis of marine food webs [1]. They also play a vital role on the carbon cycling. Through photosynthesis, phytoplankton absorb CO_2 and fix it into organic matter, which can be stored in the deep ocean or used by other organisms, helping mitigate the effects of climate change. However, phytoplankton can also have negative impacts. Harmful algal blooms (HABs) are a natural phenomenon occurring in all coastal systems, whose frequency and spatial distribution has been suggested to increase as a consequence of climate change and eutrophication [2]. Some HABs are developed by species capable of producing toxins, others are non-toxic but with high biomass proliferations that can lead to water discolouration and oxygen depletion. These events can take place in large or small areas, depending on the species and external conditions. According to UNESCO, about 300 species of microalgae have potential to form blooms, and approximately one fourth of these species are capable of producing toxins [3]. The most important producers of phytoplankton toxins are dinoflagellates and pennate diatoms. Toxic HABs are most commonly associated with three groups of toxins in Europe: paralytic toxins (PSP or paralytic shellfish poisoning) and lipophilic toxins (DSP or diarrhetic shellfish poisoning) produced by dinoflagellates, and domoic acid (ASP or amnesic shellfish poisoning) produced by pennate diatoms [4]. The threshold for harmful algae blooms (HABs) varies depending on the specific microalgae species involved and their associated toxins, and on other factors such as the location of the bloom and the properties of the ecosystem. For some microalgae species, even relatively low cell concentrations can result in harmful effects due to the potent toxins they produce. In contrast, other species may need to reach much higher cell densities before they become problematic. For instance, in Ría de Vigo, the presence of toxins in bivalves has been detected for concentrations of *Pseudo-nitzschia* species slightly above 10^5 cell per litre. For some dinoflagellates the concentration can be much lower. *Alexandrium* species and *Gymnodinium catenatum* only needs a minimum concentration around 10^3 and 10^4 cell per litre, and for *Dinophysis* species, the presence of toxins in bivalves has been detected in concentrations below 10^3 cells per litre [4]. Many studies have shown that the most common cause of PSP outbreaks is

* Corresponding authors at: CMEMS-UMinho, University of Minho, Campus de Azurém, 4800-058 Guimarães, Portugal.
E-mail addresses: vpinto@dei.uminho.pt (V. Pinto), esuarez@uvigo.gal (E. Fernández), gminas@dei.uminho.pt (G. Minas).

https://doi.org/10.1016/j.algal.2023.103317
Received 22 September 2023; Received in revised form 3 November 2023; Accepted 7 November 2023
Available online 15 November 2023

caused by dinoflagellates of the genus *Alexandrium*, and HABs from this species appears to be increasing in frequency and distribution [5–7]. Therefore, the efficient and timely monitoring of these dinoflagellates is essential to safeguard shellfish and finfish aquaculture and public health [2]. HABs monitoring programs usually include toxic phytoplankton detection as well as the presence of toxins in shellfish to inform on the closure and opening of shellfish harvesting areas. The need to acquire high resolution data on the presence of harmful phytoplankton species both on space and time, led to the development of some commercial automated devices, such as FlowCAM, CytoBuoy, Imaging FlowCytobot or Laser Optical Plankton Counter. Nevertheless, they are generally bulky and expensive [8,9]. The development of low cost, more portable and autonomous devices for HABs monitoring is thus vital and highly demanded to expand HABs monitoring programs [10–12]. With the increase in computing power, scientists have been able to develop computer models that simulate the behaviour of complex systems such as the growth and spread of phytoplankton in aquatic environments. These models, combined with satellite and in situ data on environmental conditions such as temperature, nutrients, and water currents, have been used as predictive tools to identify when and where HABs are likely to occur [13,14]. Recent advances in machine learning (ML) and deep learning (DL) have improved the accuracy, speed, affordability, and real-time monitoring capabilities of these models when used in conjunction with other monitoring techniques such as sensor networks on floating platforms or buoys [15]. By combining all of these techniques, it is possible to obtain a better understanding of the dynamics of phytoplankton growth and the occurrence of HABs, and ultimately improve our ability to predict and prevent these events. However, the detection of microalgae and more specific, early HABs by affordable in situ sensors presents some challenges due to the high diversity of phytoplankton communities and to the often low concentrations of toxic microalgae species present in seawater.

The separation of microalgae based on cell size prior to analysis is important to focus the analysis to a specific range of species and reduce the complexity of seawater samples, and the capacity to increase cell concentration before in situ measurements can be important to detect toxic species even during pre-bloom conditions. The size range of the well-known harmful algal dinoflagellate species such as *Alexandrium*, *Karenia*, and *Dinophysis* are mostly between 20 and 60 μm in size. A significant portion of species of various microalgal groups, including *Chlorophyta*, *Cryptophyta*, *Haptophyta*, *Ochrophyta*, and *Cyanobacteria*, presents smaller cell sizes (<20 μm). Despite the significant diversity of species within each group, the size difference between the larger potential harmful dinoflagellates and other smaller species can be explored to improve detection and monitoring of these dinoflagellates in the seawater.

1.1. Spiral inertial microfluidics

Inertial microfluidics are a promising and versatile approach for size-based cell separation and enrichment and has seen many progresses in the last years, exploring new channel geometries, multiplexing strategies and integration with other technologies [16–19]. The spiral microchannel is a popular design for inertial sorting as it explores intrinsic hydrodynamic forces during fluid flow to achieve particles separation, offers ease of operation, simplicity in the microfabrication process, low clogging issues, and scalability for macro-scale volume processing [20].

In curved microchannels, the interplay of the inertial lift force (F_L) and of the Dean drag force (F_D) is responsible for the inertial migration and separation of particles. These forces are illustrated in Fig. 1. The parabolic profile of fluid velocity within the microchannel, with maximum velocity at the centre and minimum velocity adjacent to the walls, results in a variation of fluid velocity across the channel's cross-section. This velocity gradient induces the shear gradient-induced lift force (F_{LS}), which acts to push particles away from the central axis of the microchannel. Simultaneously, the interaction of particles with the channels walls leads to the formation of a wall-induced lift force (F_{LW}), which exerts a pushing effect on particles, moving them away from the channel walls and towards the central region (Fig. 1a). These two forces

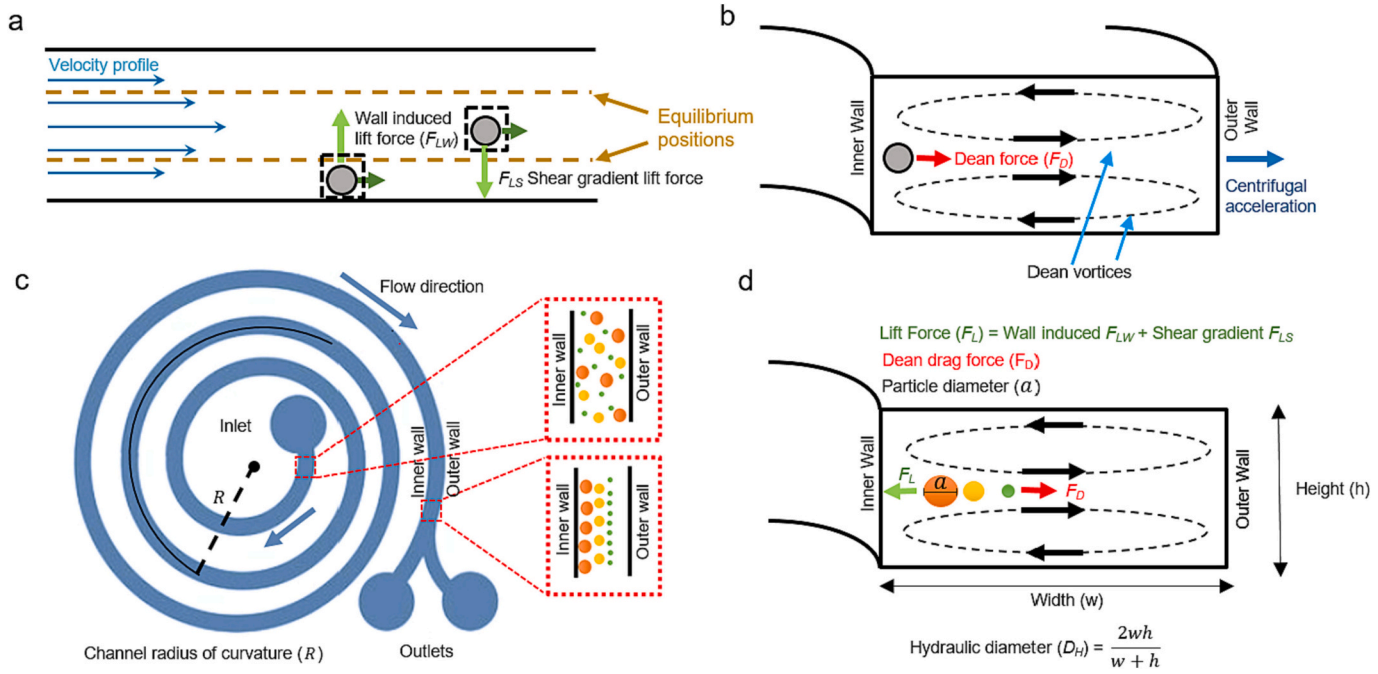

Fig. 1. a) (Top view parallel to flow direction) Representation of the net inertial lift forces composed by the shear gradient induced lift force and wall induced lift force (blue arrows represent the parabolic nature of the velocity profile) and b) (channel cross-section view perpendicular to flow direction) the Dean drag force in curved channels; c) schematic representation of the equilibrium position of different sized particles along the spiral and d) microchannel cross section showing the interaction between the net lift force (F_L) and the Dean drag force (F_D). (For interpretation of the references to colour in this figure legend, the reader is referred to the web version of this article.)

compose the net lift forces (F_L). In curved microchannels, the combination of pressure-driven flow and centrifugal forces originates the formation of secondary flow patterns known as Dean flows. Dean flows are characterized by two symmetrical counter-rotating vortices formed at the top and at the bottom of the cross-sectional plane of the microchannel. These Dean flows exert a Dean drag force (F_D) on the particles, pushing them towards the centre and outer wall of the channel (Fig. 1b). The magnitude of Dean flow can be characterized by the dimensionless Dean number (*De*)

$$De = Re\sqrt{\frac{D_H}{2R}} = \frac{\rho U D_H}{\mu}\sqrt{\frac{D_H}{2R}} \quad (1)$$

where *Re* is the channel Reynolds number which describes the ratio of inertial forces to viscous forces, D_H is the hydraulic diameter, R is the channel radius of curvature, ρ is the fluid density, U represents the mean velocity flowing in the microchannel and μ is the viscosity.

Flowing particles might encounter additional forces, like viscous drag, buoyancy, and centrifugal forces, but these forces are negligible and can be disregarded in this context. A ratio (R_F) between the net lift forces and Dean drag force can then be defined to estimate the competition between these forces

$$R_F = \frac{F_L}{F_D} = \frac{2R \cdot a^2}{D_H^3} f \quad (2)$$

where a is the particle diameter, and f is a dimensionless function that ranges from 0.02 to 0.03 at channel Reynolds numbers of between 20 and 95 [21]. This comparison offers a simple way to determine how particles will behave according to the magnitude of the ratio, completely carried along in the secondary flow when the ratio is much smaller than 1; unaltered by the secondary flow when the ratio is higher than 1, or settling into an equilibrium between the two forces when the ratio is approximately equal to 1. The particle confinement ratio (*CR*) and flow rate are the most important parameters for focusing and for lateral migration of particles [22]. *CR* can be defined as *a/Dh* [23], where "*a*" is the particle diameter and "*Dh*" the microchannel hydraulic diameter. For moderate flow rates ($De < 75$) three flowing modes can be described based on *CR* values [24]. For $CR > 0.07$, which is a reference value found in literature for the inertial focusing of particles in curved channels, the particles are in the focusing mode. Here, they occupy a well-defined position in the channel, usually near the inner wall. A $CR > 0.07$ means the lift forces are dominant and responsible for the particles' equilibrium within the microchannel. For $0.01 < CR < 0.07$, the particles enter the rough focusing mode, where they form a broader distribution band in the microchannel. For $CR < 0.01$, the particles enter the un-focusing mode, where they are randomly distributed across the channel, independent of the flow rate.

The influence of the main forces (F_D and F_L) on the particles is affected by the particles size. The interplay between these two dominant forces creates an equilibrium position for the particles along the channel width. Large particles where inertial lift forces are more predominant focus closer to the inner wall, while smaller particles more influenced by Dean drag forces and less affected by inertial lift forces will focus further away from the inner wall (Fig. 1c, d). Since flow conditions and channel geometries can affect the shape and magnitude of Dean vortices, these parameters can be tuned to enhance microfluidics cell sorting capabilities [25]. For instance, in rectangular spiral microchannels, as the channel height increases, particles experience less shear-induced inertial forces and more Dean drag forces. In the same way, a smaller curvature radius of the channel also implies stronger Dean forces, shifting the focused particle streams away from the inner wall. An increased aspect ratio (width/height) of the channel cross-section results in a greater separation distance between particles of different sizes, thereby enhancing the effectiveness of separation [26].

When a given velocity threshold is surpassed, the Dean forces begin to dominate over the inertial forces resulting in de-focusing of the particles stream [27] and the inertial focusing ceases to exist. Very small particles ($a/Dh \ll 0.07$), where the inertial forces are negligible to focus the particles trajectories, undergoes lateral migration through the microchannel in the form of oscillations back and forth the channel width. This migration is termed Dean Cycle and this phenomenon can also be explored to achieve separation of microparticles [28]. The simplicity of fabrication, implementation, and high throughput makes this method suitable for integration in lab-on-a-chip (LOC) devices. This focusing principle does not require sheath flows and has low risk of clogging issues, making it ideal for long term monitoring. Studies also demonstrate that cells are not significantly affected by the high flow and shear rates in inertial microfluidic systems [29].

Thus, in this work it is studied and developed a simple inertial microfluidic device, based on a double spiral microchannel, for size-separation and concentration of microparticles/microalgae. First, different microparticles sizes and microalgae species were used to validate the focusing principle and the possibility of manipulating the trajectory by varying the flow velocity. The capabilities for separation and enrichment of non-toxic and toxic microalgae were confirmed by fluorescence measurements and particle tracking at the outlets.

2. Materials and methods

2.1. Channels microfabrication

Spiral microchannels were fabricated in polydimethylsiloxane (PDMS), with 300 μm width and 100 μm height. The geometry uses double spiral channels with a total of 10 loops and length of approximately 20 cm, with one inlet and two outlets (see Section 3.1 for the geometry selection).

The microfluidic structure was crafted from PDMS (Polydimethylsiloxane) via soft lithography, using a SU-8 photosensitive resin (SU-8 100) fabricated through a cost-effective UV photolithography process, established in our research laboratory, eliminating the need for cleanroom facilities, [30]. The PDMS fabrication follows standard fabrication steps, which details, including the SU-8 mold, are described in supplementary material S1.

2.2. Particle tracking

The trajectory of particles and cells within the microchannels was experimentally validated using the Nemesys Syringe Pump with its coupled software interface, allowing the inlet of fluids with high precision and controlled flow rates. For visualization, it was used an inverted microscope (IX71, Olympus, Tokyo, Japan) connected to a high-speed camera to capture the movement of particles/cells.

In order to facilitate the visualization of the particles' trajectory as they exit through the outlets, a particle tracking algorithm was developed in MATLAB. The particle tracking process started with a video captured in the final portion of the spiral, closer to the outlets, with the high-speed camera. The frames were processed with MATLAB software. Each frame was subtracted to the previous frame and converted to binary. The result is an image where all the background and static elements are turned into black pixels and the moving objects are turned into white pixels. Filters were included in the process to eliminate noise. The moving objects correspond to particles moving towards the exit. The white pixels positioning around the width of the microchannel were saved in an array at each frame subtraction. This process was repeated for all frames and a final plot showing the accumulated position of particles regarding to the width of the channels was obtained. A smooth processing (Lowess) was applied to the data for the plots.

2.3. Microparticles and microalgae preparation

Particle suspensions were prepared by diluting polystyrene (PS) microparticles with dimensions of 6, 10, 20 and 40 μm in distilled water.

Microalgae cultures of *Alexandrium tamarense*, *Alexandrium minutum*, *Rhodomonas lens*, and *Tetraselmis suecica* were obtained from the ECIMAT microalgae collection and kept in 250 ml Erlenmeyer flasks and in an incubation chamber at a temperature of ±18 °C and under illumination of fluorescent lamps with a cycle of 10 h light and 14 h dark.

2.4. Fluorescence analysis

After sorting and enrichment tests, microalgae samples collected at the spiral outlets were placed in quartz cuvettes. An optical fiber was connected to the bottom of the cuvette adapter in a 90-degree angle with the excitation LEDs (Light Emitting Diodes). Microalgae fluorescence was determined using the 450 nm excitation LED as a light source. For the separation tests (Section 3.3), a 540 nm excitation LED was used instead. Both LEDs are part of the ams OSRAM Polychromatic LuxiGen Multi-Color LED (LZ7-A4M2PD-0000) from Mouser electronics. The fluorescence signal at the 570–800 nm region was collected by the portable spectrophotometer (AvaSpec-ULS2048x64-EVO by Avantes), through an optical fiber, and recorded in a laptop. The fluorescence signal intensity was used to estimate chlorophyll *a* concentrations, as it's a commonly used indicator of phytoplankton biomass. A smooth processing (Lowess) was applied to the data for the plots.

3. Results and discussion

3.1. Microparticles and microalgae focusing and distribution at the outlets

To seek the inertial focusing and separation capabilities of microparticles and microalgae, PS microparticles with 6, 10, 20 and 40 μm sizes and 4 species of microalgae were selected for the experimental tests. PS microparticles possess well-defined and precise sizes, enabling us to assess the system's performance and its capacity to sort and focus particles of varying dimensions. This evaluation was crucial for comprehending how effectively our microfluidic setup handles particles of different sizes, ultimately validating our chosen methodology and experimental setup and providing a solid foundation for microalgae experimental tests. The dimensions of the selected species are represented in Fig. 2a. These dimensions were calculated through analysis of microscopic images. Fig. 2b shows the side scattering (SSC) and forward scattering (FSC) of *Alexandrium minutum* (1945 cell events), *Alexandrium tamarense* (638 cell events), *Tetraselmis suecica* (3821 cell events) and *Rhodomonas lens* (33,053 cell events). The flow cytometry adds more robustness to the morphologic comparison between species, since it analyses a bigger population of cells when compared to the morphologic analysis of microscopic image. The FSC measures the intensity of light scattered in the forward direction, and correlates to the size of cells, that means, the bigger the cells the higher the forward scattered light. SSC measures the intensity of light scattered at a 90-degree angle from the laser beam, and relates to the granularity or internal complexity of cells. Thus, more complex the cell, more scattered light to the sides. Microscopic images of the species are shown in Fig. 2c. Both microalgae measured through optical microscopy and by flow cytometry seem to be in agreement, with a clearly morphological distinction between the *Alexandrium* genus and the remaining species, with both *Alexandrium* species being considerably bigger in size.

The various solutions of suspended microparticles and microalgae were injected one at a time in the microfluidic chip with varying velocities. The microfluidic microchannel presents a double spiral geometry, so it has a total of ten loops, and while the focusing effect is dependent on both spiral channels, the separation effect is only dependent on the second spiral channel (Fig. 3a). Double channel spirals can be engineered to optimize the separation efficiency between particles of different sizes [24], but in this work the main reason of the double spiral is to take advantage of the larger channel length and extra curves to potentiate the desegregation of cell conglomerates, since many species can form long chains that can potentially clog the microchannel.

The channel dimensions of 300 μm width and 100 μm height were selected to accommodate the desired particle size range, which falls

a

Species	Shape	Size Mean ± SD (number of cells)
Alexandrium tamarense	Sphere	Diameter: 29.18 ± 4.3 μm (21)
Alexandrium minutum	Sphere	Diameter: 20.15 ± 2.2 μm (32)
Tetraselmis suecica	Oval	Long axis: 11.55 ± 1.46 μm (29)
Rhodomonas lens	Oval	Long axis: 10.49 ± 0.86 μm (24)

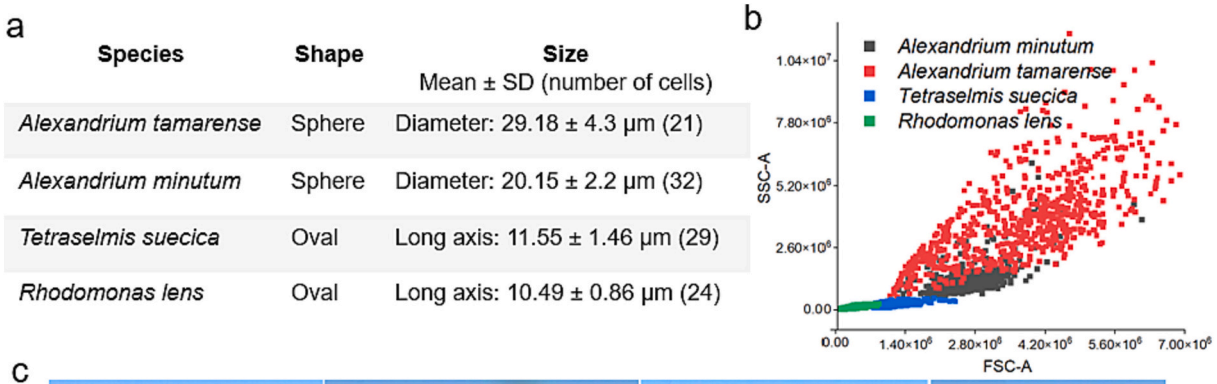

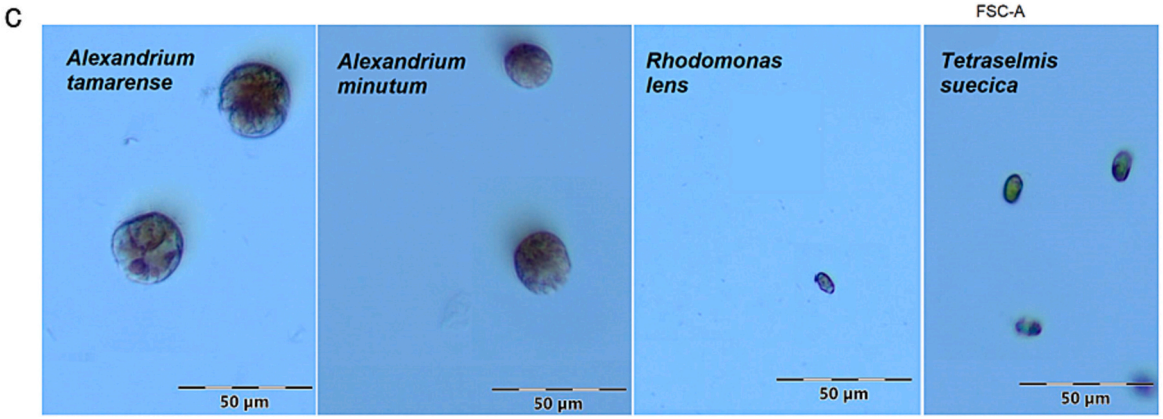

Fig. 2. a) Shape and dimensions of the selected species used in the experimental tests; b) forward scattering and side scattering of microalgae species; c) microscope images of microalgae species (scale bar 50 μm).

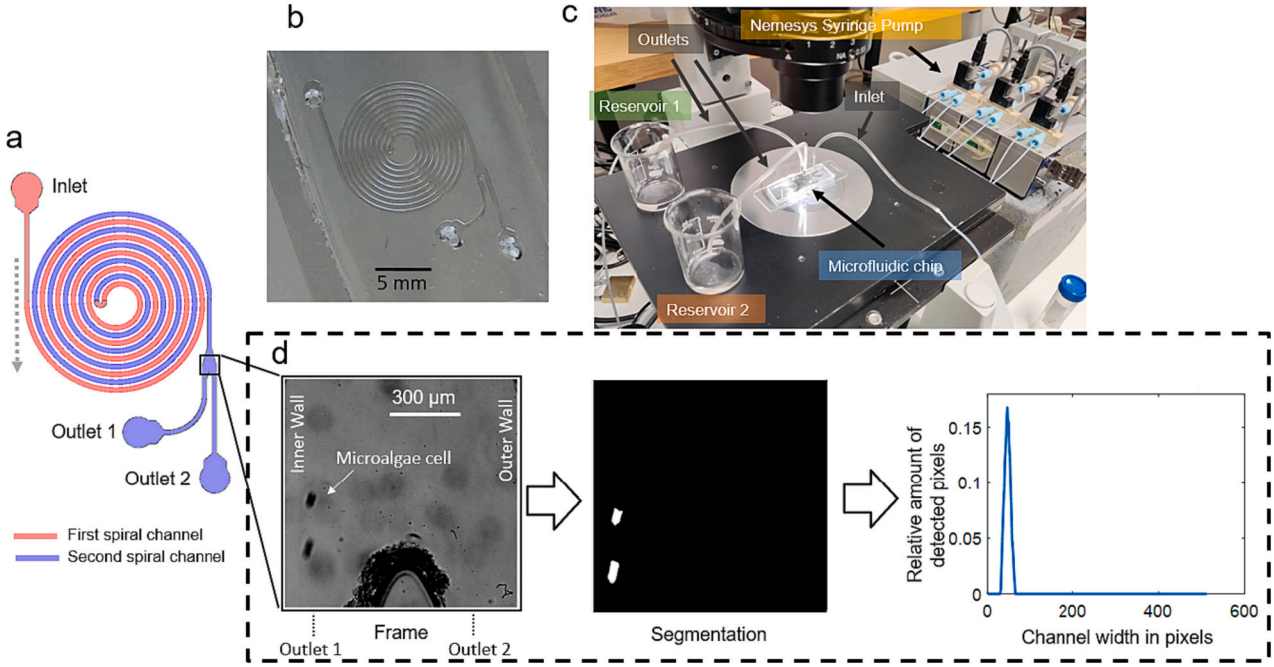

Fig. 3. a) Design of the double spiral; b) PDMS microfluidic spiral; c) experimental setup; d) particle tracking using MATLAB. (Left) First frame showing two cells of *Alexandrium tamarense* moving towards the outlets. (Center) The result of the subtraction between two consecutive frames with filters applied to remove unwanted noise. The white pixels correspond to the moving objects. (Right) Plot showing the position of the cells along the width of the microchannel.

within the 10 µm to 40 µm range, encompassing the size of microalgae cells studied in this work. The selection was guided by the condition $a/D_h > 0.07$, meaning that particles with a minimum diameter of approximately 10 µm can effectively focus inertially within the channel ($D_h = 150$ µm). An aspect ratio of 3 was chosen for these channels. While a higher aspect ratio does promote improved separation between particles of different sizes, it was also demonstrated that as the channel's geometric aspect ratio increases, the equilibrium particle focusing streak widens [31]. Therefore, a balance must be met in selecting a proper channel cross section dimension that achieves the intended goal of both effective separation and maintaining a well-focused particle stream, allowing for better control and concentration of particles.

The flow rates for outlet 1 and for outlet 2 are relatively equal, e.g. for a flow rate of 2000 µl/min at the inlet, we have ~1000 µl/min at each outlet despite some minor fluctuations that do not have impact in the final results. So, each outlet as a recovery rate of 50 % approximately. Various flow rates were tested starting from 800 µl/min up to 3400 µl/min ($De \approx 20$–100).

A PDMS double spiral is presented in Fig. 3b. The microparticles/cells trajectories were recorded with a high-speed camera coupled with the optic microscope aimed at the outlets region. The microalgae were then collected into two reservoirs, one for each outlet (Fig. 3c). Fig. 3d shows the main steps for particles tracking at the end portion of the spiral.

The results from the tracking algorithm for PS microparticles with various sizes and the microalgae (*Tetraselmis suecica* and *Alexandrium minutum*) are presented in Fig. 4. The tracking algorithm analysed 2000 frames of video captured at 5000 fps. In almost all the microparticles tested with the different flow rates, a well-defined position was observed at the outlets region. However, the 6 µm microparticles show dispersed positions along the channel width. The 6 µm microparticles are well below 0.07 but still above 0.01 (CR = 0.04), so they are in the rough focusing mode. Despite that, those particles displayed an unfocused behaviour, being distributed across all the channel, regardless of the flow rate. For the remaining particles and microalgae, the ratio is ≥0.07, and they all acquire relatively well-defined trajectories at the spiral outlets. It can also be observed a trajectory shift of the microparticles in direction to the outer wall of the channel with increasing flow rate. This is expected because while the particle focusing mode is mainly attributed to the CR value, that is, the ratio between particles and channel cross-section size, the position and width of the particles trajectory in the channel width can be, largely, determined and manipulated by the flow rate [22]. For 10 µm particles, the transition from outlet 1 to outlet 2 starts to take shape at around 2000 µl/min. In the case of 20 µm microparticles, an increase in flow rate to 2600 µl/min promotes the transition from outlet 1 to outlet 2. The larger 40 µm microparticles remained in the path to outlet 1 for all tested flows. It's worth noting that the 40 µm microparticles seemingly showed unexpected results between 800 µl/min and 2000 µl/min, i.e., the trajectory position moved closer to the inner wall as velocity increased within that range. One possible explanation might be attributed to the increase of inertial forces with higher flow rate, which naturally pushes the particles closer to the inner wall, while the dean forces despite also increasing with higher velocities, remain very weak for relatively large particles and for that reason do not exert much influence on the 40 µm particles. For smaller particles (i.e., 10 µm), the inertial forces are less dominant and in turn they are more influenced by the Dean drag forces, for that reason, they move easier towards the microchannel outer wall. Overall, these results are in agreement with previous findings showing that large particles are expected to focus closer to the inner wall, where the inertial lift forces are stronger, while smaller particles will focus further away from the inner wall. An increase in the flow rate also shifts the smaller particles further away from the inner wall, while larger particles are less affected and their trajectory shift is less pronounced.

The same principles are applied to microalgae. Our tested cultures of *Tetraselmis suecica* and *Alexandrium minutum* have sizes around 12 µm and 20 µm, respectively. The trajectory shift was more substantial for *Tetraselmis suecica* than with *Alexandrium minutum*. Since *Tetraselmis suecica* cells are smaller, they move more easily towards the outer wall and their transition from outlet 1 to outlet 2 starts around 2600 µl/min. For *Alexandrium minutum*, the trajectory split between both outlets at around 3000 µl/min. Taking into account the positions of the microparticles/microalgae for different flow velocities, it is possible to obtain separation with an appropriate design of the spiral channel geometry

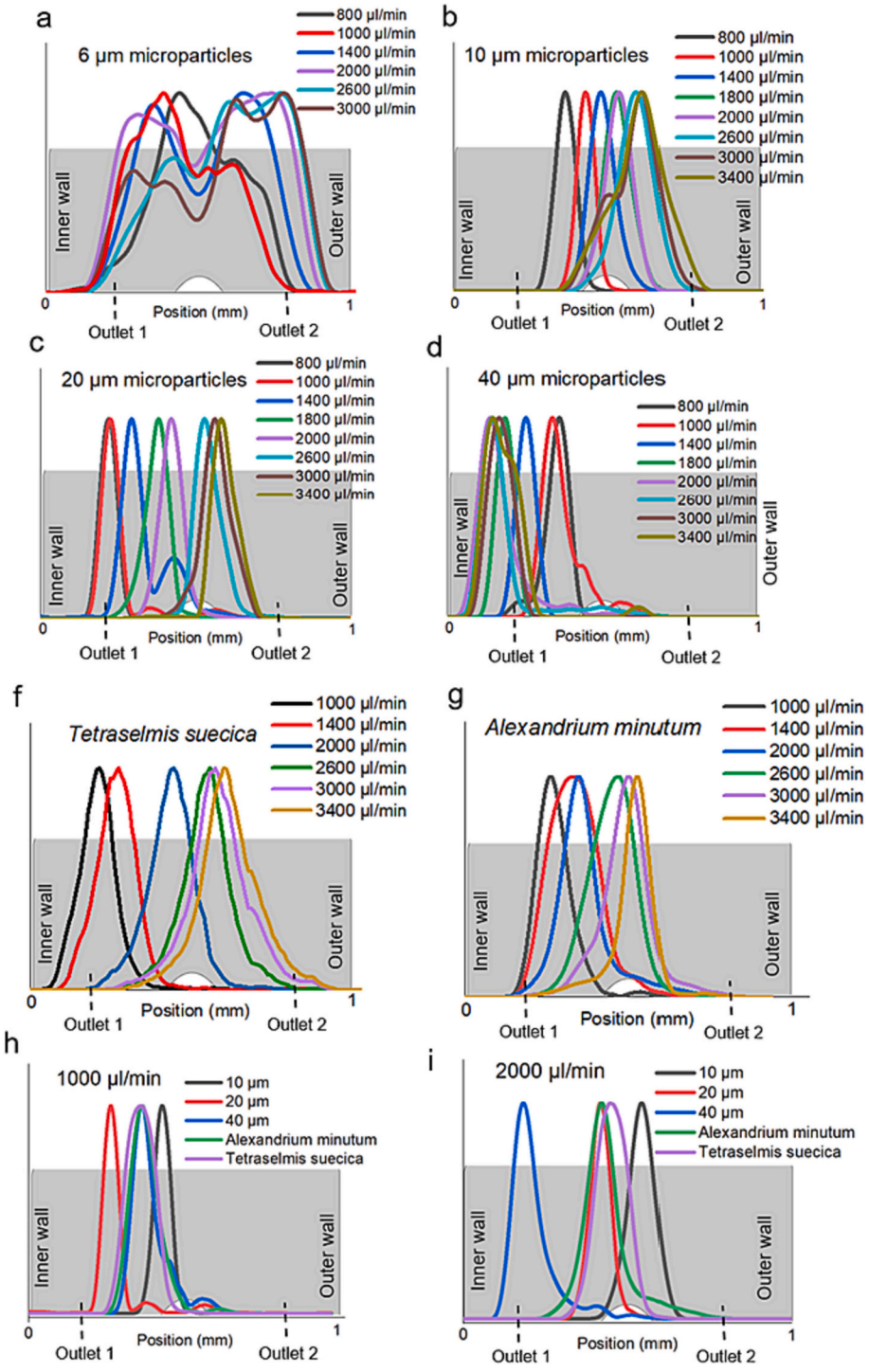

Fig. 4. Position for PS microparticles of a) 6 µm; b) 10 µm; c) 20 µm; and d) 40 µm, f) *Tetraselmis suecica* and g) *Alexandrium minutum*, at the outlets for various flow rates, and position of microparticles and microalgae for fixed flow rates of h) 1000 µl/min and i) 2000 µl/min.

and outlets, and the size-based particles separation can be tuned by varying the flow velocity. For improved results, the spirals must be tailored for the species of interest, as the CR plays a crucial role in the microalgae focusing mode that has direct impact on the performance of the device, whether to isolate, concentrate or remove one or more species from a sample.

3.2. Cell concentration

Fluorescence is a very sensitive and specific method for detecting microalgae. The fluorescence intensity of microalgae is often proportional to their concentration. Chlorophyll-a is the primary photosynthetic pigment in microalgae and emits fluorescence in the 680 nm region, being commonly used as an indicator of phytoplankton biomass. Furthermore, considering that different microalgae species have different fluorescence signatures, fluorescence signals can be utilized to distinguish different microalgae species. As fluorescence techniques are usually non-destructive, the microalgae cells are not damaged during the measuring procedure. Fluorescence is also a relatively inexpensive, accurate and simple technique, being widely employed to monitor

microalgae populations [15]. In order to detect microalgae using fluorescence, the concentration of microalgae in the sample must be high enough to produce a detectable fluorescence signal. Thus, the pre-enrichment of target microalgae can be used to increase the emitted fluorescence signal, and consequently, the sensitivity of the device. To validate the concentration capacity of microalgae samples using spiral inertial microfluidics, a solution of *Tetraselmis suecica* was introduced in the spiral with a flow rate of 1400 μl/min. This chosen flow rate took into account the size of this microalgae species and the effectiveness for their navigation in the microfluidic channels and focus at outlet 1 while also expediting the testing process. The outputted solutions of both outlets were excited with a LED centred at 450 nm and their fluorescence intensity was measured in the range of 680 nm (see Section 2.4). The concentrated solution at outlet 1 was again introduced into the same spiral for a 2nd cycle and the fluorescence emitted by both solutions at the outlets was measured again. The enrichment process is demonstrated in Fig. 5a, which shows a visual representation of *Tetraselmis suecica* tracking using video frames captured by the high speed camera coupled with the optic microscope. Here, a simplified version using only 200 frames is shown, with the normalized tracking plot showing the position of microalgae detected along the width of the channel, and an image frame with an overlayed binary image of the accumulated microalgae in green colour for a more intuitive visualization. Fig. 5b displays the fluorescence signal increase at the outlet 1 after both cycles and sign shows a more complete tracking using 2000 frames, and without normalization to highlight the difference between the particles detected in the 1st and in the 2nd cycle. The particle tracking plot hints that the majority of cells exit towards the first outlet, and the curve magnitude from the 1st to the 2nd cycle increases, meaning that more particles are detected at the 2nd cycle. The samples collected at outlet 1 and outlet 2 for both cycles can be seen in Fig. 5c, where a greenish colour is visible at outlet 1 while outlet 2 presents a more transparent aspect.

For the initial diluted culture, the fluorescence peak measured was at around 9400 units. After the 1st cycle through the spiral, the fluorescence intensity peak of the concentrated solution at outlet 1 was measured at approximately 14,500 units, a 1.55-fold increase in relation to the initial solution. At the 2nd cycle, the fluorescence intensity peak reached around 21,200 units, representing a 1.46-fold increase in the emitted fluorescence intensity between the first and second cycle. After 2 cycles, the sample had a total increase of 2.3-fold in fluorescence peak signal when compared to the initial diluted solution (Fig. 5d). At the outlet 2, in both cycles, the fluorescence measurement was around 2400 units. Because the detected fluorescence intensity is proportional to the concentration of microalgae in the sample, the increase in the fluorescence signal at outlet 1 after both cycles, along with a significant decrease at outlet 2, confirms a clear concentration rise of Tetraselmis suecica (Fig. 5e).

The same experimental procedure was employed for *Alexandrium minutum* (Fig. 6), one of the main dinoflagellates responsible for toxic HABs, but this time, the initial culture of *Alexandrium minutum* was diluted until only a faint fluorescence signal was detected, and the sample was subjected to tree cycles in the spiral. Now, the chosen flow rate was 2000 μl/min, due to the larger size of this microalgae species. This flow proved to be suitable for achieving a good trajectory focus of *Alexandrium minutum* towards outlet 1, while minimizing the duration of the tests. In Fig. 6a, the visual representation of cells tracking using 200 frames shows *Alexandrium minutum* cells focused closer to the inner wall of the spiral, exiting through outlet 1, as expected. The tracking plot with 2000 frames analysed for each of the 3 cycles (Fig. 6b) confirms the majority of cells position towards outlet 1, and an increase in cell detection after each cycle. This is in agreement with the observed colour difference of the samples collected at both outlets (Fig. 6c). The collected sample at outlets 1 from each cycle had a yellow brown colouration, typical of dinoflagellates, while the samples collected at the outlets 2 were more transparent. The fluorescence results confirmed the concentration of *Alexandrium minutum*, with a 2.4-fold increase in the emitted fluorescence peak between the initial diluted concentration (~1757 units) and the 1st cycle (~4270 units), a 1.7-fold increase between the 1st and 2nd cycle (~7110 units) and a 1.4-fold increase between the 2nd and 3rd cycle (~10,135 units) (Fig. 6d). The emitted fluorescence in outlet 2 decreased significantly, staying bellow ~1800 units in all cycles. When comparing the fluorescence peak of the initial diluted samples with the concentrated sample after 3 cycles, it is observed an increase in fluorescence peak signal of 5.8-fold (Fig. 6e).

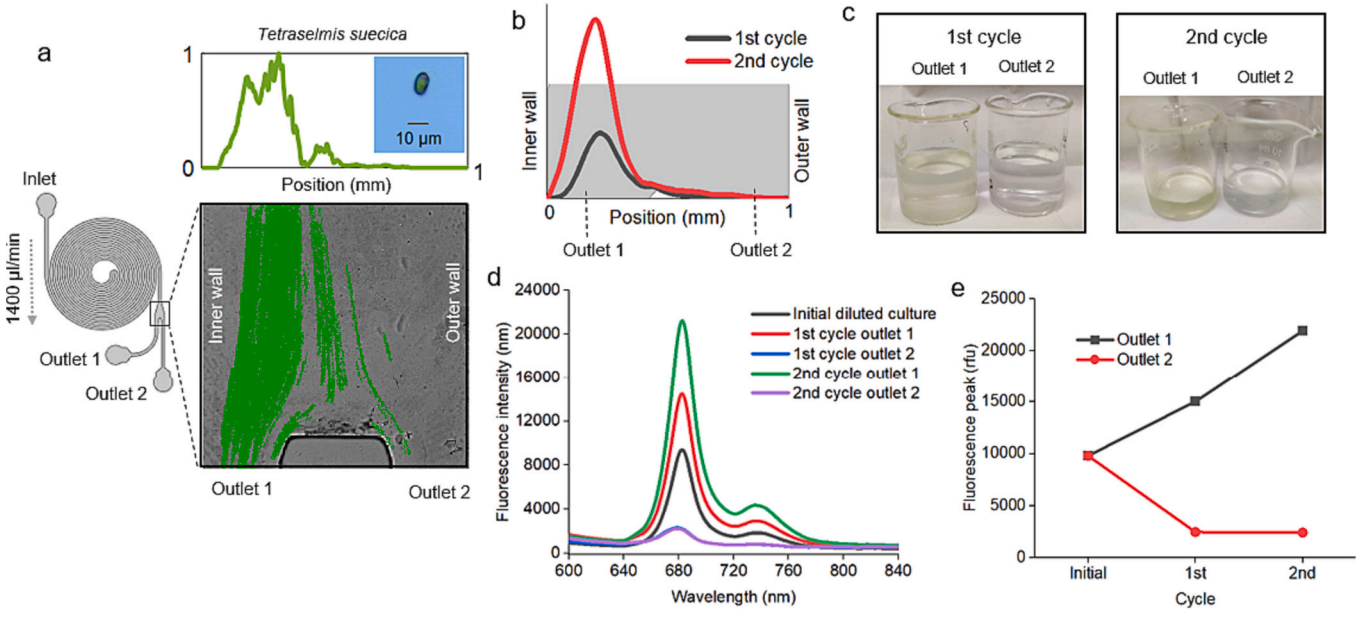

Fig. 5. Enrichment method for *Tetraselmis suecica* with 2cycles in the spiral. a) Visual representation of *Tetraselmis suecica* tracking at the outlet region of the spiral; b) *Tetraselmis suecica* trajectory at the outlets for the 1st and 2nd cycle; c) *Tetraselmis suecica* solutions collected at each outlet; d) fluorescence emission spectrum excited at 450 nm for each cycle and e) plot comparing the peak fluorescence signal at each outlet for all cycles.

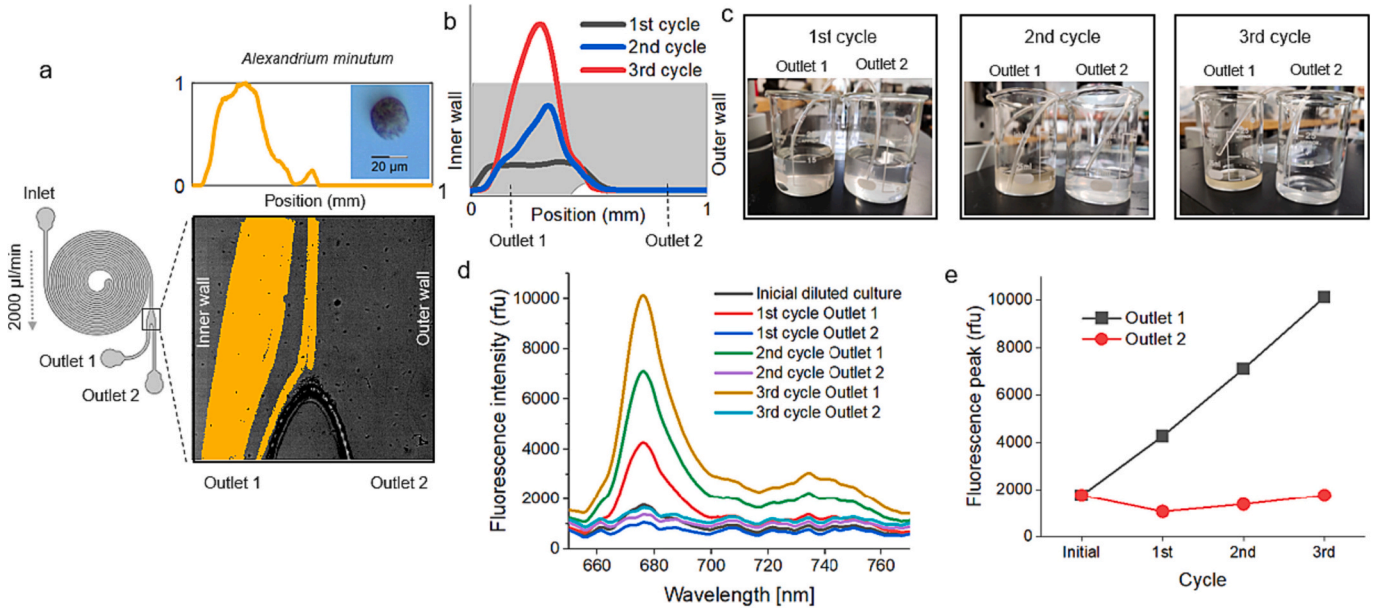

Fig. 6. Enrichment method for *Alexandrium minutum* with 3 cycles in the spiral. a) Visual representation of *Alexandrium minutum* tracking at the outlet region of the spiral; b) *Alexandrium minutum* trajectory at the outlets for the 1st, 2nd and 3rd cycle; c) *Alexandrium minutum* solutions collected at each outlet; d) fluorescence emission spectrum excited at 450 nm for each cycle and e) plot comparing the peak fluorescence signal at each outlet for all cycles.

3.3. Species separation in mixtures

Seawater samples are made of a complex interaction between various microalgae populations. The ability to isolate certain species of interest from natural samples can be extremely important to facilitate its identification. For example, the ability to identify toxic species can be improved by targeting their size to achieve isolation from other microalgae species, followed by enrichment, which increases the chances of

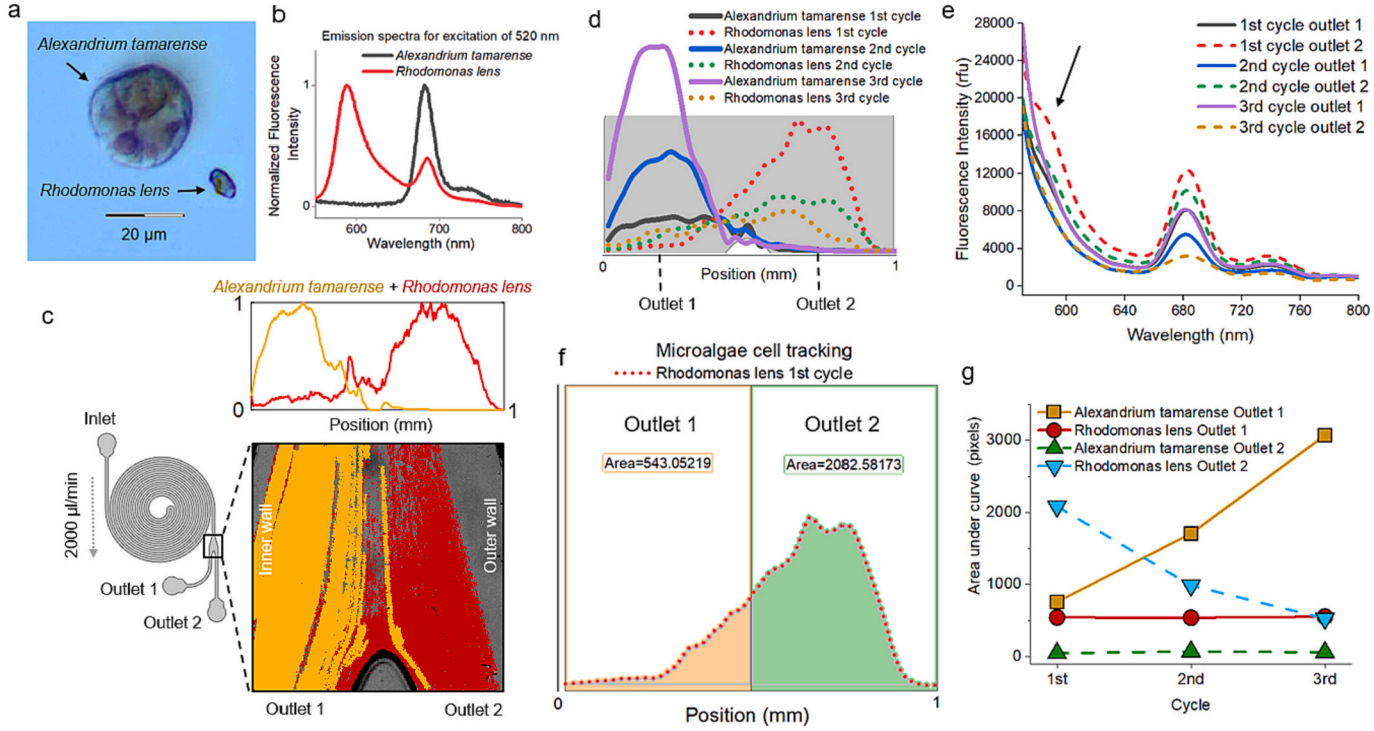

Fig. 7. a) Microscope image showing a size comparison between *Alexandrium tamarense* (yellow) and *Rhodomonas lens* (red) (bar scale = 20 µm); b) normalized emission spectra excited at 520 nm for *Alexandrium tamarense* and *Rhodomonas lens*. c) Visual representation of *Alexandrium tamarense* and *Rhodomonas lens* tracking at the outlet region of the spiral; d) *Alexandrium tamarense* and *Rhodomonas lens* trajectory at the outlets for the 3 cycles; e) Fluorescence emission spectrum excited at 520 nm for the sample mixture. f) Method to obtain the degree of isolation of species using the area under curve of the tracking plot of panel d. In this case, an example showing the *Rhodomonas lens* split between both outlets for the 1st cycle (details in Fig. S2 of section S3 of supplementary material); g) graph comparing the normalized area distribution under the curve at each outlet for both species across the 3 cycles. (For interpretation of the references to colour in this figure legend, the reader is referred to the web version of this article.)

detection. To test this assumption, a mixture of cultures of *Alexandrium tamarense* and *Rhodomonas lens* was used (Fig. 7).

Alexandrium tamarense is a potentially toxic dinoflagellate and *Rhodomonas lens* is a Cryptophyte. *Alexandrium tamarense* and *Rhodomonas lens* have significantly different sizes, with the *Alexandrium tamarense* cultures displaying an average size around 30 μm and the *Rhodomonas lens* around 10 μm (Fig. 7a). Furthermore, *Rhodomonas lens* has the pigment phycoerythrin, which is not present in the dinoflagellate *Alexandrium*. This pigment is excited between 500 and 560 nm and emits fluorescence at 585 nm. Fig. 7b shows the normalized emission spectrum with excitation at 520 nm for *Alexandrium tamarense* and *Rhodomonas lens*. Both species show a peak emission at around 680 nm, but *Rhodomonas lens* has a distinctive peak at around 585 nm. This means the two selected species have distinct sizes and spectral signatures, making them ideal candidates to test the separation capabilities of the microfluidic spiral. Indeed, these were the reasons to choose these species for the separation tests instead of the previously tested *Alexandrium minutum* and *Tetraselmis suecica* in single-species experiments (as demonstrated in Figs. 4, 5, and 6). While *Tetraselmis suecica* has a different pigment composition compared to *Alexandrium* species, both emit fluorescence at the same region of the spectrum (around 680 nm), making it challenging to distinguish the separation based on fluorescence data. Therefore, *Rhodomonas lens* was chosen instead of *Tetraselmis suecica*. The *Alexandrium tamarense* choice relied on its high average size (of 30 μm) when compared to *Alexandrium minutum* (of 20 μm), allowing to exhibit a clearer and more effective separation from the small-sized *Rhodomonas lens*, maximizing the separation capabilities of the spiral within our specific spiral configuration (the results of Fig. 4, even using PS microparticles, allowed this conclusion). It's important to emphasize that the omission of *Alexandrium minutum* in this specific test does not imply its incapacity for separation.

A flow of 2000 μl/min was chosen to achieve isolation of *Alexandrium tamarense* from *Rhodomonas lens* with 3 cycles in the spiral. As shown in Fig. 7c, *Alexandrium tamarense* maintains a trajectory confined to the inner wall of the channel, exiting mostly through outlet 1, while *Rhodomonas lens* presents a broader distribution and is located closer to the centre and outer wall of the channel. The data processing is similar to that shown in Figs. 5a and 6a, but here we track both species of different sizes by adjusting the threshold values in separate variables for each species, resulting in a final image frame with two overlayed binary images, yellow colour representing *Alexandrium tamarense* and red colour for *Rhodomonas lens*, highlighting their preferential trajectories at the outlets (the algorithm that represents the object tracking and the visual representation at the outlet region of the spiral is included in S2 supplementary material). The cell tracking of *Alexandrium tamarense* and *Rhodomonas lens* is presented in Fig. 7d. The algorithm filters were adjusted to detect *Alexandrium tamarense* cells and *Rhodomonas lens* cells in the mixture in separated steps. A separation in the trajectories of both species is clearly noticeable, with an increase in the number of *Alexandrium tamarense* cells detected with each cycle, while *Rhodomonas lens* cells number decreased. Fig. 7e shows the fluorescence signal of the samples collected at the outlets for 3 cycles when excited with a 540 nm LED. Besides the fluorescence peak at 680 nm, characteristic of chlorophyll *a*, there is also a protuberance between 580 and 590 nm indicated by a black arrow, which corresponds to the phycoerythrin pigment present in *Rhodomonas lens*. This bump at around 585 nm increases for the sample collected at the outlet 2 of the 1st cycle (red dashed line), and decreases for the sample collected at the outlet 1 of the 1st cycle (black line). This means that in outlet 1 the presence of *Rhodomonas lens* is reduced, while its presence in outlet 2 is reinforced. The sample collected at the outlet 1 was reintroduced for the 2nd cycle, and at the outlet 1 the protuberance in the region of 585 nm practically disappeared (blue line), while at outlet 2 there was an increase of that protuberance (green dashed line), indicating a greater isolation between both species at the end of the 2nd cycle. A decrease in the peak at 680 nm is also observed for both samples collected at the outlet 1 of the first 2 cycles, compared to the samples collected at the outlet 2. This is observed because *Rhodomonas lens* is responsible for the highest fluorescence emission, and despite the increase in *Alexandrium tamarense* concentration in the outlet 1, the amount of *Rhodomonas lens* removed from these samples results in a net loss of fluorescence intensity at 680 nm. At the 3rd cycle it is observed an increase in the fluorescence signal at the 680 nm region at the outlet 1, and a fluorescence decrease for the same region at outlet 2. These results suggest the 3rd cycle contributed mainly for the concentration of *Alexandrium tamarense* as most of the separation between species was done in the first 2 cycles.

As we are dealing with a mixture of two species, and since there is fluorescence overlap between the two species, it is difficult to obtain relative quantitative data through fluorescence signals to assess the separation of both species in the sample. For a more deeper analysis, the tracking graph of Fig. 7d was split in half along the x-axis, where the channel width is represented (Fig. 7f). It was then assumed that the microalgae detected in the left half (orange) exited through outlet 1 and the microalgae detected in the right half (green) exited towards outlet 2. The area under the curve (orange for microalgae exiting through outlet 1 and green for outlet 2) was calculated separately for each half of the plot (of Fig. 7d), in order to have a numerical value that would allow us to evaluate, in a relative way, the degree of isolation of the species in each cycle through the spiral. The area units are in pixels since the curves indicates how many pixels contribute to the detected object at that particular position (more details are in supplementary material S3). The results obtained are represented as a plot in Fig. 7g. We can't directly compare the value magnitude of the cell tracking between *Alexandrium tamarense* and *Rhodomonas lens*, as one cell of *Alexandrium tamarense* represents much more pixels detected than a cell of *Rhodomonas lens* (see Fig. 4d). However, the increase and decrease in magnitude for each species after each cycle gives valuable information to assess the behaviour of both species in the spiral. By looking at the plot we can easily observe a substantial growth of detected *Alexandrium tamarense* as the sample was subjected to the 3 cycles, with a 2.2-fold increase between the first and the 2nd cycle, and a 4-fold increase between the 1st and the 3rd cycle. At the same time, the amount of *Alexandrium tamarense* cells that came out of outlet 2 was extremely small, representing only a 5.6 % loss of cells for the 1st cycle, a 4 % loss for the 2nd cycle and a loss of 1.9 % for the 3rd cycle. For *Rhodomonas lens*, 20.7 % and 79.3 % of the detected cells exited through outlet 1 and 2 of the 1st cycle, respectively. For the 2nd cycle, the distribution was split between 35.3 % for outlet 1 and 64.7 % for outlet 2. At the 3rd spiral, the distribution between both outlets evened out with 51.2 % and 48.8 % for outlet 1 and 2, respectively. The highest percentage of *Rhodomonas lens* came out in outlet 2 of the 1st cycle. This relative percentage decreased for the second spiral because the sample that entered the 2nd cycle was collected from outlet 1 of the first cycle, so it was expected that the number of *Rhodomonas lens* would decrease. As the mixture flows throughout the cycles, smaller species of *Rhodomonas lens*, which are more difficult to focus in a stable trajectory, get distributed between both outlets, which might explain why *Rhodomonas lens* are evenly distributed across the two outlets at the 3rd cycle, as the larger *Rhodomonas lens* species were removed in the first and second spirals. The cell tracking results match the fluorescence plots and confirm the separation and isolation capabilities of microfluidic spirals for species of different sizes in mixtures.

3.4. Continuous method for size-based isolation and enrichment

The recirculation in the spiral presents very good results. It is suitable for laboratory use and it can also be used outside the laboratory, since it can easily be made into a compact unit with just a few components (syringe pumps, microfluidic system, tubing, reservoirs). However, it has some drawbacks that needs to be addressed. First, it is limited by the initial volume of sample available. For a spiral with two outlets, both with the same output flow velocity, the volume collected at each outlet

will decrease roughly by half at each recirculation. So, the number of possible cycles will depend on the available initial volume. Second, it presents some difficulties to fully integrate into an in-situ system that, for instance, operates autonomously underwater (for instance, coupled with a sensor for continuous monitoring of seawater blooms). One way to achieve this is through the arrangement of spirals in series. In this case, the enrichment capacity would be defined by the number of spirals in series. Nonetheless, this would add more complexity, higher pressure and higher risk of clogging. To try to overcome these limitations, an alternative system is suggested. A scheme for continuous sample enrichment was developed that achieves gradual increase of microalgae concentration. The tested configuration consisted of a microfluidic chip, two micropumps (model RP-QII & RP-QIII Series from the supplier BMT Fluid Control Solutions GmbH), an electronic control system (ZK-J5X step down power supply module) to adjust the micropump flow rate and two reservoirs. A schematic representation of the system is shown in Fig. 8a. In this scheme two micropumps were used at the same time. Micropump 1 (RP-QIII) pumps the sample into the spiral and micropump 2 (RP-QII) returns the sample, that exit through the outlet 1, back into the spiral. The working principle is the following: with the appropriate flow rate in the two micropumps, microparticles or microalgae with sizes of interest will exit through outlet 1 towards reservoir 1, and then reintroduced into the spiral, exiting again at outlet 1, remaining "trapped" in the system. As micropump 1 pushes more sample into the spiral, more microparticles/microalgae in the size range of interest are trapped in the system, and as a result, the sample concentration will increase in reservoir 1. In theory, this increase in concentration will be proportional to the operating time of the system.

A diluted culture of *Alexandrium minutum* was used for the experimental test. The pumping rate of micropump 1 and micropump 2 was around 800 µl/min. The cell tracking at the outlets and the fluorescence measurements at the reservoir 1 are plotted in time intervals of 20 min (Fig. 8b, c). The system running time was 80 min. The position of detected cells demonstrates the majority of microalgae exiting at the outlet 1 throughout the whole running time. The fluorescence measurement results confirmed the concentration of *Alexandrium minutum*, with a fluorescence peak increase between 1.2 and 1.4-fold at intervals of 20 min, and a total of 2.85-fold increase after 80 min of operation (Fig. 8d). This continuous method presents a slower concentration compared with the previous cycles' method of Section 3.3 (Fig. 8f). However, while slower in its capability to concentrate, it is not constrained by a fixed initial volume and subsequently number of cycles, and rather relies on the time of operation to increase concentration. It should be noted that since we used peristaltic micropumps for this experiment, the flow velocity presents a slightly pulsed behaviour, making it less precise and less stable when compared with the Nemesys syringe pump used in the cycle method (Section 3.2), which might have a slight influence in the presented results. This biggest pro of the continuous method rely, in theory, on the analysis of an infinite volume of sample, being limited either by clogging problems, particle saturation, biofouling or component failure. It is also easy to integrate in an in-situ system as its main components are 1 spiral and 2 micropumps. The low energetic consumption of micropumps allows this mechanism to operate autonomously for long periods of time. The feasibility of this system underwater might be possible but more experimental tests are needed to understand the effect of pressure from the water and the closed microfluidic loop on the performance of this method.

One of the biggest challenges of the spiral inertial microfluidics in seawater monitoring is the scalability of this technology. The system must be scalable to handle larger volumes efficiently. For that, increase throughput is need, reducing the time required to process larger quantities of samples. This scale-up can be done through multiplexing/parallelisation of several microfluidic spiral. This was already demonstrated by previous works, such as by Miller et al. [32], achieving an impressive throughput of 1 l/min using a stack of 20 microfluidic devices [32] and future work must be addressed in this particular topic.

The main aim of the device is to facilitate and improve the detection using available methods, giving them the ability to detect samples of low concentrations through selective pre-enrichment before measurements. Additionally, the separated cells from potentially toxic species can be

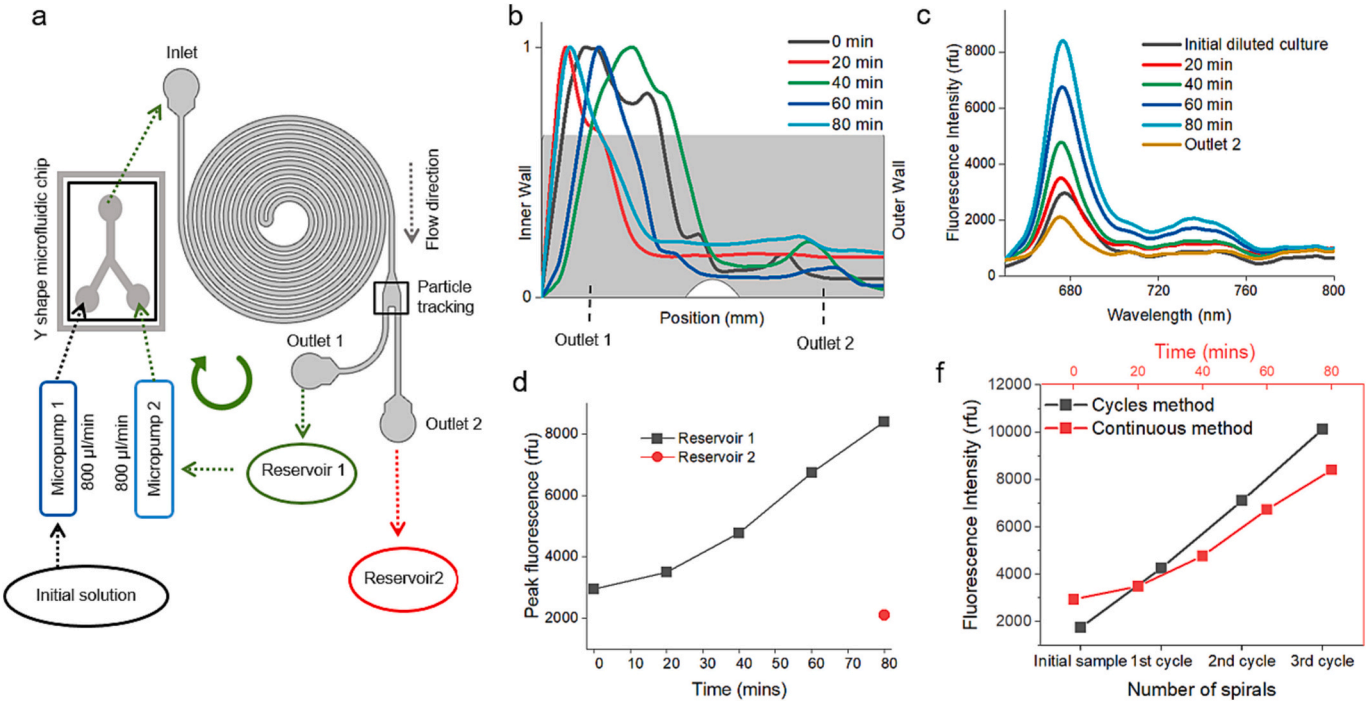

Fig. 8. *Alexandrium minutum* enrichment with continuous method. a) scheme demonstrating the process for continuous enrichment of *Alexandrium minutum*. b) *Alexandrium minutum* normalized trajectory at the outlets in intervals of 20 min; c) fluorescence emission spectrum excited at 450 nm; d) plot comparing the peak fluorescence signal at each reservoir at the 680 nm region. Reservoir 1 shows fluorescence measures in intervals of 20 min, while reservoir 2 shows the measured fluorescence after 80 min; f) comparison between fluorescence peak at 680 nm for the cycles method (Section 3.3) and for the single spiral continuous method.

properly stored and discarded after treatment.

The characteristic larger size of toxic dinoflagellates compared to most non-toxic species makes them candidates for separation and concentration before analysis, not only reducing sample complexity by removing cell sizes outside the scope of interest, but also by providing concentration of cells in the detection module, as identifying early stages of toxic blooms requires the capability to detect very few cells per litter. Implementing cell concentration before analysis is an ingenious approach to enhance available methods without using more expensive equipment or components, thus maintaining the device low cost. An in situ sensor using this enrichment method can be designed to continuously sample seawater for an extended period of time, thus considerably increasing cell concentrations inside a size range of interest, and allowing the detection of very few cells per litre, and trigger warnings for HABs in early stages.

4. Conclusions

This work successfully developed a simple inertial microfluidic spiral device for size-based microalgae separation and concentration. The device showed effectiveness in sorting microalgae of different sizes and modulating separation based on flow velocity. It demonstrated a significant increase in microalgae concentration, e.g., a 5.8-fold increase in *Alexandrium minutum* fluorescence after 3 cycles. It also effectively isolated and enriched *Alexandrium tamarense* in a mixture with *Rhodomonas lens with* cell losses below 6 %. The use of spiral inertial microfluidics for isolation and concentration of toxic dinoflagellates for better HABs detection and monitoring offers a unique approach of this technology for environmental monitoring.

CRediT authorship contribution statement

Conceptualization, Vitor Magalhães, Vânia Pinto and Paulo Sousa; Data curation, Vitor Magalhães, Vânia Pinto, Emilio Fernández; Formal analysis, Luís Gonçalves, Emilio Fernández and Graça Minas; Funding acquisition, Vânia Pinto and Luís Gonçalves; Investigation, Vitor Magalhães, Vânia Pinto and Paulo Sousa; Methodology, Vitor Magalhães, Vânia Pinto and Emilio Fernández; Supervision, Vânia Pinto and Emilio Fernández; Validation, Luís Gonçalves, Emilio Fernández and Graça Minas; Roles/Writing – original draft, Vitor Magalhães, Vânia Pinto and Paulo Sousa; Writing – review & editing, Luís Gonçalves, Emilio Fernández and Graça Minas.

All authors have read and agreed to the published version of the manuscript.

Declaration of competing interest

The authors declare that they have no known competing financial interests or personal relationships that could have appeared to influence the work reported in this paper.

Data availability

No data was used for the research described in the article.

Acknowledgements

This work has been supported by the project Eye-on-shell (EXPL/EAM-OCE/1155/2021), and partially supported by the project PlastiSensor (PTDC/EAM-OCE/6797/2020), through national funds (OE), within the scope of the Scientific Research and Technological Development Projects (IC&DT) program in all scientific domains (PTDC), through the Foundation for Science and Technology, I.P. (FCT, I.P). Work was also partially supported by the European Union's Horizon 2020 research and innovation programme via ASSEMBLE Plus under grant agreement No 730984, and under the national support to R&D units grant, through the reference project UIDB/04436/2020 and UIDP/04436/2020. V.M. thanks the FCT for the PD/BD/150581/2020 grant. V.P. thanks FCT for her contract funding provided through 2021.01087.CEECIND and P.S. thanks FCT for his contract funding provided through 2021.01086.CEECIND.

Appendix A. Supplementary data

Supplementary data to this article can be found online at https://doi.org/10.1016/j.algal.2023.103317.

References

[1] R.J. Geider, E.H. Delucia, P.G. Falkowski, A.C. Finzi, J.P. Grime, J. Grace, F. I. Woodward, Primary productivity of planet earth: biological determinants and physical constraints in terrestrial and aquatic habitats, Glob. Chang. Biol. 7 (8) (2001) 849–882.

[2] P. Lassus, N. Chaumérat, P. Hess, E. Nézan, Toxic and Harmful Microalgae of the World Ocean, International Society for the Study of Harmful Algae and the United Nations Educational, Scientific and Cultural Organisation, 2015.

[3] UNESCO IOC Harmful Algal Bloom Programme, What are harmful algae? Harmful Algal Bloom Programme website, Retrieved from, https://hab.ioc-unesco.org/what-are-harmful-algae/, 2023, July 10.

[4] B.R. Ramírez, L. Escalera, Y.P. González, Á. Moroño, Episodios de fitoplancton tóxico en la Ría de Vigo, in: La Ría de Vigo: una aproximación integral al ecosistema marino de la Ría de Vigo, Instituto de Estudios Vigueses, 2008, pp. 153–199.

[5] K. Hayes, C. Sliwa, S. Migus, F. McEnnulty, P. Dunstan, National priority pests: part II ranking of Australian marine pests, in: An Independent Report Undertaken for the Department of Environment and Heritage by CSIRO Marine Research, 2005, pp. 1–106.

[6] S.C.Y. Leong, A. Murata, Y. Nagashima, S. Taguchi, Variability in toxicity of the dinoflagellate Alexandrium tamarense in response to different nitrogen sources and concentrations, Toxicon 43 (4) (2004) 407–415.

[7] C. Zou, R.M. Ye, J.W. Zheng, Z.H. Luo, H.F. Gu, W.D. Yang, J.S. Liu, Molecular phylogeny and PSP toxin profile of the Alexandrium tamarense species complex along the coast of China, Mar. Pollut. Bull. 89 (1–2) (2014) 209–219.

[8] S. Dunker, D. Boho, J. Wäldchen, P. Mäder, Combining high-throughput imaging flow cytometry and deep learning for efficient species and life-cycle stage identification of phytoplankton, BMC Ecol. 18 (1) (2018) 1–15.

[9] Z. Göröcs, M. Tamamitsu, V. Bianco, P. Wolf, S. Roy, K. Shindo, A. Ozcan, A deep learning-enabled portable imaging flow cytometer for cost-effective, high-throughput, and label-free analysis of natural water samples, Light: Sci. Appl. 7 (1) (2018) 1–12.

[10] D.A. Carvalho, V.C. Pinto, P.J. Sousa, V.H. Magalhães, E. Fernández, P.A. Gomes, L. M. Gonçalves, Methodology for phytoplankton taxonomic group identification towards the development of a lab-on-a-chip, Appl. Sci. 12 (11) (2022) 5376.

[11] L. Zeng, D. Li, Development of in situ sensors for chlorophyll concentration measurement, J. Sensors 2015 (2015) 1–16.

[12] S.E. Zieger, G. Mistlberger, L. Troi, A. Lang, F. Confalonieri, I. Klimant, Compact and low-cost fluorescence based flow-through analyzer for early-stage classification of potentially toxic algae and in situ semiquantification, Environ. Sci. Technol. 52 (13) (2018) 7399–7408.

[13] I. Caballero, R. Fernández, O.M. Escalante, L. Mamán, G. Navarro, New capabilities of Sentinel-2A/B satellites combined with in situ data for monitoring small harmful algal blooms in complex coastal waters, Sci. Rep. 10 (1) (2020) 1–14.

[14] P.J. Franks, Recent advances in modelling of harmful algal blooms, in: Global Ecology and Oceanography of Harmful Algal Blooms, 2018, pp. 359–377.

[15] A. Mozo, J. Morón-López, S. Vakaruk, Á.G. Pompa-Pernía, Á. González-Prieto, J.A. P. Aguilar, J.M. Ortiz, Chlorophyll soft-sensor based on machine learning models for algal bloom predictions, Sci. Rep. 12 (1) (2022) 13529.

[16] D. Huang, J. Man, D. Jiang, J. Zhao, N. Xiang, Inertial microfluidics: recent advances, Electrophoresis 41 (24) (2020) 2166–2187.

[17] N. Xiang, Z. Ni, Inertial microfluidics: current status, challenges, and future opportunities, Lab Chip 22 (24) (2022) 4792–4804.

[18] X. Xu, X. Huang, J. Sun, R. Wang, J. Yao, W. Han, M. Yin, Recent progress of inertial microfluidic-based cell separation, Analyst 146 (23) (2021) 7070–7086.

[19] Z. Zhou, Y. Chen, S. Zhu, L. Liu, Z. Ni, N. Xiang, Inertial microfluidics for high-throughput cell analysis and detection: a review, Analyst 146 (20) (2021) 6064–6083.

[20] N. Liu, C. Petchakup, H.M. Tay, K.H.H. Li, H.W. Hou, Spiral inertial microfluidics for cell separation and biomedical applications, in: Applications of Microfluidic Systems in Biology and Medicine, 2019, pp. 99–150.

[21] D.R. Gossett, D.D. Carlo, Particle focusing mechanisms in curving confined flows, Anal. Chem. 81 (20) (2009) 8459–8465.

[22] N. Xiang, Z. Shi, W. Tang, D. Huang, X. Zhang, Z. Ni, Improved understanding of particle migration modes in spiral inertial microfluidic devices, RSC Adv. 5 (94) (2015) 77264–77273.

[23] S.S. Kuntaegowdanahalli, A.A.S. Bhagat, G. Kumar, I. Papautsky, Inertial microfluidics for continuous particle separation in spiral microchannels, Lab Chip 9 (20) (2009) 2973–2980.

[24] H. Jeon, B. Jundi, K. Choi, H. Ryu, B.D. Levy, G. Lim, J. Han, Fully-automated and field-deployable blood leukocyte separation platform using multi-dimensional double spiral (MDDS) inertial microfluidics, Lab Chip 20 (19) (2020) 3612–3624.
[25] N. Xiang, K. Chen, D. Sun, S. Wang, H. Yi, Z. Ni, Quantitative characterization of the focusing process and dynamic behavior of differently sized microparticles in a spiral microchannel, Microfluid. Nanofluid. 14 (1) (2013) 89–99.
[26] C. Liu, C. Xue, X. Chen, L. Shan, Y. Tian, G. Hu, Size-based separation of particles and cells utilizing viscoelastic effects in straight microchannels, Anal. Chem. 87 (12) (2015) 6041–6048.
[27] D. Di Carlo, Inertial microfluidics, Lab Chip 9 (21) (2009) 3038–3046.
[28] H.W. Hou, M.E. Warkiani, B.L. Khoo, Z.R. Li, R.A. Soo, D.S.W. Tan, C.T. Lim, Isolation and retrieval of circulating tumor cells using centrifugal forces, Sci. Rep. 3 (1) (2013) 1259.
[29] M.S. Syed, M. Rafeie, D. Vandamme, M. Asadnia, R. Henderson, R.A. Taylor, M. E. Warkiani, Selective separation of microalgae cells using inertial microfluidics, Bioresour. Technol. 252 (2018) 91–99.
[30] V.C. Pinto, P.J. Sousa, V.F. Cardoso, G. Minas, Optimized SU-8 processing for low-cost microstructures fabrication without cleanroom facilities, Micromachines 5 (3) (2014) 738–755.
[31] A.E. Reece, J. Oakey, Long-range forces affecting equilibrium inertial focusing behavior in straight high aspect ratio microfluidic channels, Phys. Fluids 28 (4) (2016).
[32] B. Miller, M. Jimenez, H. Bridle, Cascading and parallelising curvilinear inertial focusing systems for high volume, wide size distribution, separation and concentration of particles, Sci. Rep. 6 (1) (2016) 36386.